Terahertz imaging using a high-$T_c$ superconducting Josephson junction detector



2008 Supercond. Sci. Technol. 21 125025

(http://iopscience.iop.org/0953-2048/21/12/125025)

Supercond. Sci. Technol. **21** (2008) 125025 (5pp) doi:10.1088/0953-2048/21/12/125025

# Terahertz imaging using a high-$T_c$ superconducting Josephson junction detector

**J Du[1], A D Hellicar[2], L Li[2], S M Hanham[2], N Nikolic[2], J C Macfarlane[1] and K E Leslie[1]**

[1] CSIRO Materials Science and Engineering, PO Box 218, Lindfield NSW 2070, Australia
[2] CSIRO ICT Centre, PO Box 76, Epping NSW 1710, Australia

E-mail: Jia.Du@csiro.au and Andrew.Hellicar@csiro.au

Received 11 August 2008, in final form 8 October 2008
Published 7 November 2008
Online at stacks.iop.org/SUST/21/125025

**Abstract**

A high-$T_c$ superconducting (HTS) detector based on a $YBa_2Cu_3O_{7-x}$ (YBCO) step-edge Josephson junction has been developed and applied to terahertz (THz) detection. The detector was coupled to a ring-slot antenna designed for operation at 600 GHz, and used for THz imaging. The results suggest that the characteristic voltage and frequency of our HTS step-edge junctions can be readily optimized for the chosen THz frequency range at easily achievable temperatures. The images also clearly demonstrate some of the unique properties of THz radiation, including the sensitivity to water content and the ability to penetrate packaging materials.

(Some figures in this article are in colour only in the electronic version)

## 1. Introduction

Terahertz waves (300–3000 GHz) have many unique properties, such as strong sensitivity to water content, high transmission through a range of plastics, fabrics, and paper materials, and spectroscopic responses to many materials [1]. These features mean THz waves are applicable to non-destructive imaging or inspection of numerous materials, including explosives, drugs, and hidden objects, and medical imaging and diagnosis. Despite huge prospects, widespread application of THz systems has been delayed due to limitations of the available source and detector technologies. Developing new THz sources, detectors and imaging systems is a subject of great current interest.

Detectors with high sensitivity, wide-band frequency coverage and large arrays are required for THz imaging. Semiconductor bolometers [2] have been widely used as sensitive cryogenic detectors of THz waves but they are extremely sensitive to temperature fluctuation, mechanical vibration and electrical interference, and the performance deteriorates with increasing frequencies in the THz range. Superconducting devices are excellent candidates due to their distinctive advantages of extremely low noise, low power consumption and high frequency operation (well into the THz band). Luukanen *et al* [3, 4] developed low-temperature superconducting (LTS) Nb microbolometers and obtained passive THz images for security screening. Ariyoshi *et al* [5, 6] developed a Nb tunnel junction detector and acquired transmission THz images at very low temperatures (0.3 K). Detectors based on Nb technology can only operate at liquid helium temperatures (4.2 K or below) and the tunnel junction detectors have an upper frequency limit of ∼1 THz (due to a gap voltage of ∼2.8 meV). High-temperature superconducting (HTS) devices can operate at higher temperatures, which reduce cryogenic costs, and have a higher energy gap than LTS devices, giving response frequencies well into the THz range. The energy gap of YBCO ranges from 10 to 60 meV [7], corresponding to a gap frequency of 5–30 THz. There have been a few demonstrations of THz frequency detection based on HTS bicrystal junctions [8–13]; the highest detected frequency is ∼4.25 THz [12]. However, imaging at THz frequencies with HTS Josephson junction detectors has not, to our knowledge, been reported, although a demonstration of mm-wave imaging using an HTS ramp junction was reported [14].

In this work, we propose and demonstrate an HTS Josephson detector for THz imaging. The aim is to develop

 

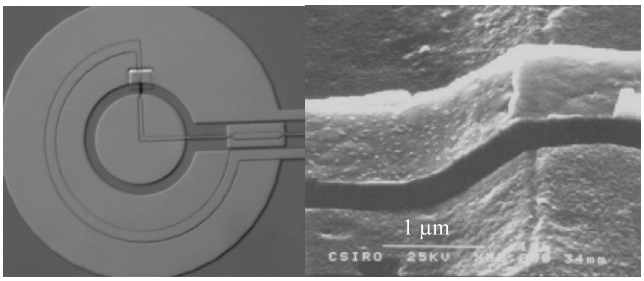


**Figure 1.** (Left) Micrograph of the fabricated ring-slot antenna-coupled superconducting Josephson detector (the YBCO junction is located in the upper part of the circular slot), and (right) a close-up view of the step-edge Josephson junction. The YBCO microstrip line underneath the gold antenna shown in the left photo is for the dc biasing of the junction.

a practical and compact real-time THz video camera with a detector being able to work at temperatures well above liquid helium temperatures, so that cooling can be provided by a relatively cheap commercial cryocooler. Our HTS YBCO step-edge junction technology [15, 16] is well placed to make such a detector as its characteristic voltage and, therefore, characteristic frequency can be tailored to some degree for high frequency applications. It also has the flexibility to allow the junction to be placed anywhere on the chip and is suitable for building an array of detectors. As a proof of the concept, we have obtained the first images with a single HTS step-edge Josephson junction detector coupled with a thin-film ring-slot antenna.

## 2. Device fabrication and DC $I$–$V$ characterization

The devices are based on the established step-edge YBCO junction technology developed at CSIRO [15, 16]. The MgO substrates were first angle-etched using Ar-ion beam milling to produce steps of ∼400 nm height and an angle of ∼35° normal to the substrate surface in the desired positions. The YBCO films of 200–220 nm with a 50 nm *in situ* gold film were deposited by Theva GmbH. Josephson junctions of ∼2 $\mu$m wide were then patterned using a standard photolithography technique. An additional gold layer was then deposited using a dc magnetron sputtering technique for the contact pads and the antenna structures. The total gold film was chosen to be 300 nm for the designed antenna. A layer of 50 nm *in situ* gold on YBCO ensures a low contact resistance [17] for both the contact pads and the antenna.

Figure 1 shows micrographs of the fabricated antenna-coupled HTS Josephson detector and a close-up of the step-edge junction. A 2 $\mu$m wide YBCO microbridge positioned across a step on the MgO substrate forms the weak link. The junction is located across the ring-slot antenna and positioned orthogonally to a coplanar waveguide filter. The YBCO microstrip line underneath the gold antenna shown in the photo on the left is for the dc biasing of the junction. The ring-slot antenna was designed for an operation frequency of ∼0.6 THz and was chosen for its simplicity and its ability to be packed closely for an array configuration.

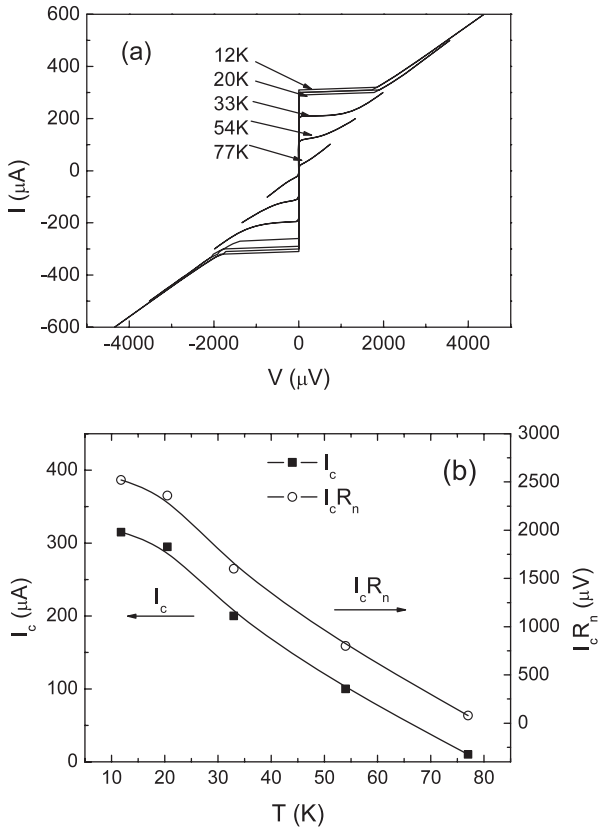


**Figure 2.** (a) DC $I$–$V$ characteristics of a step-edge junction at different temperatures ($R_n \approx 8\ \Omega$) and (b) $I_c$ and $I_cR_n$ values versus temperature.

Figure 2 shows the measured dc current–voltage ($I$–$V$) characteristics of a junction detector at different temperatures, and a graph of the junction critical current, $I_c$, and characteristic voltage, $V_c \equiv I_cR_n$, versus temperature. The junction demonstrated resistive-shunt-junction like $I$–$V$ curves with a normal resistance $R_n \sim 8\ \Omega$, determined from the linear sections of the $I$–$V$ curves. The $I_c$ value increases dramatically with decreasing temperature and, therefore, the junction characteristic voltage, $V_c \equiv I_cR_n$, and the characteristic frequency, $f_c \equiv I_cR_n/\Phi_0$ ($\Phi_0 \equiv h/2e$ is the magnetic flux quantum), are also temperature dependent. By varying the temperature, the $V_c$ and $f_c$ values can be adjusted to a large degree. A high $I_cR_n$ product is desired for Josephson junction detectors as the dynamic resistance $R_d(V) = dV/dI = R_n(V^2+V_c^2)^{1/2}/V$ and the voltage sensitivity $\eta(V) = \Delta V/P_{rf}$ (where $P_{rf}$ is the rf power coupled into the junction and $\Delta V$ is the voltage modulation amplitude induced by rf radiation) are $V_c$ dependent. For a broadband detector biased just above $I_c$, a higher $I_cR_n$ value (high $R_d$ value) should result in a larger voltage response $\Delta V$ $(V)$ for a fixed incident rf power. For the junctions used in this experiment, typical $V_c$ values are ∼100 $\mu$V at 77 K and ∼3 mV at 4.2 K, which correspond to $f_c$ values of ∼50 GHz and ∼1.5 THz, respectively. These figures show that our step-edge Josephson junctions are suitable for detecting mm, sub-mm and THz waves.

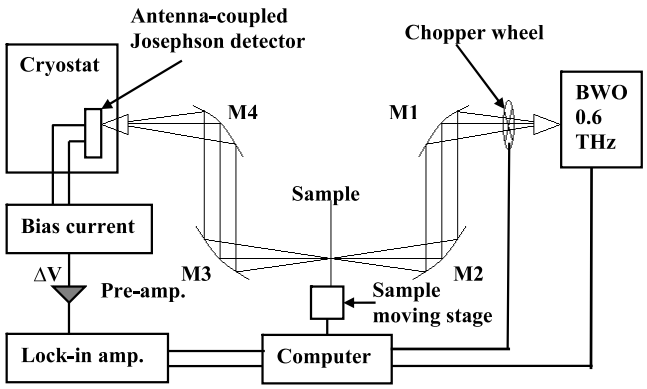


**Figure 3.** Schematic diagram of the THz transmission imaging set-up.

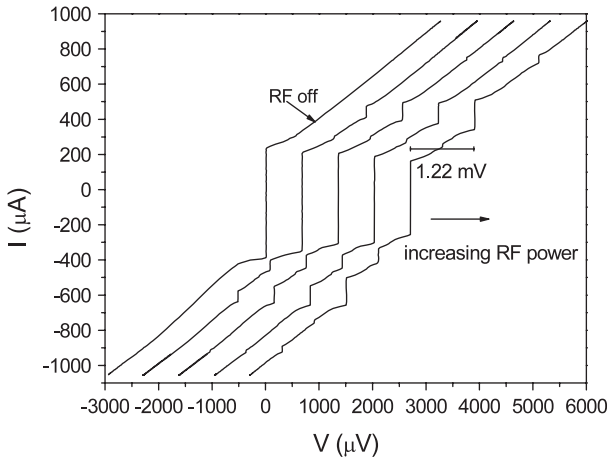


**Figure 4.** Shapiro steps on the $I$–$V$ curves for a ring-slot antenna-coupled HTS step-edge junction induced by the radiation of the 0.6 THz signal. The graphs for different rf powers are shifted horizontally for clarity. The rf power increment is 3 dB each time.

## 3. Imaging system design

The antenna-coupled HTS Josephson detector was successfully operated in an imaging mode. The system set-up [18] is shown in figure 3. A backward wave oscillator (BWO) was used to generate tuneable CW radiation around 0.6 THz. The junction and antenna were mounted on a liquid $N_2$/He cryostat and were illuminated with the THz source through a THz-transparent window on the cryostat. A quasi-optical system, comprising collimating and focusing mirrors, was used to focus the beam through the sample and then onto the detector. By translating the sample through the fixed focused point the transmission properties of the sample were able to be imaged. The spot size of the imaging system is approximately 1 mm and the typical scan resolution is 0.5 mm. The junction was dc current biased at just above $I_c$ (a sharp $dV/dI$ point on the $I$–$V$ curve shown in figure 2(a)), and the voltage response $\Delta V$ induced by the incident THz radiation was obtained and amplified by a low noise preamplifier operated at room temperature. Both the dc current source and the preamplifier were battery powered to reduce the possibility of power supply-related noise. The sample being imaged was raster scanned in a plane perpendicular to the beam axis using a linear XY motor stage. A lock-in amplifier synchronized with an optical chopper was used to acquire the voltage responses, which were processed by a computer for imaging. All measurements were performed with no added dc or rf shielding other than that provided by the aluminium cryostat housing.

## 4. Results and discussion

Figure 4 shows the frequency-selective response of one of our ring-slot antenna-coupled detectors cooled in the cryostat filled with liquid helium and illuminated with the 0.6 THz radiation source. Clear Shapiro steps were induced at the voltage $V_n = n\Phi_0 f_s = n \times (1.22\ \text{mV})$ ($n = \ldots, -2, -1, 0, 1, 2, \ldots$), where the signal frequency $f_s = 0.6$ THz. Sub-harmonic steps at half voltage steps were also observed, which are not yet fully understood. It is thought to result from the Josephson frequency mixing effect. The current step-heights, $I_n$, increase with increasing rf power (with each increment of 3 dB). The changes of the rf power were obtained by using a number of 3 dB cardboard attenuators placed in front of the cryostat window. This graph proves that our antenna-coupled step-edge junction detector responds to the applied THz radiation as predicted by the AC Josephson effect.

From the graphs, we can estimate the rf power coupled into the junction and the voltage sensitivity. The $n$th Shapiro step size is $I_n/I_c = J_n(2\ \text{eV}_{rf}/hf)$, where $V_{rf}$ is the rf voltage amplitude and $J_n(x)$ is the $n$th-order Bessel function. For example, using the current step-height $I_0$ at zero voltage, $I_0/I_c = J_0(2\ \text{eV}_{rf}/hf)$, we obtained $V_{rf} = 1.55$ mV for the $I$–$V$ curve of the maximum rf power radiation (the rightmost $I$–$V$ curve in figure 4), which corresponds to the rf power, $P_{rf} = (1/2)V_{rf}^2/R_n \approx 0.3\ \mu$W (note: $R_n = 4\ \Omega$ for this junction). Then, by differentiating the un-irradiated $I$–$V$ curve in figure 4, we obtained the dynamic resistance $R_d = dV/dI \approx 30\ \Omega$ at the device operating point. The voltage modulation amplitude $\Delta V = R_d \Delta I$, where $\Delta I$ is the induced current change, and from these observations, we estimate the voltage sensitivity $\eta = \Delta V/P_{rf} \approx 12\,000\ \text{V W}^{-1}$. Using any of the $I$–$V$ curves under different rf power levels in figure 4, similar $\eta$ values were obtained. This value is higher than that of the Schottky-diode detectors reported [19]. The rf power coupled into the junction was estimated to be less than 1% of the source power. There is a considerable amount of impedance mismatch between the antenna ($\sim$30 $\Omega$) and the junction (typically 1 to 10 $\Omega$). In our design, we positioned the junction to maximize the impedance matching. A higher $R_n$ value is desired for a better signal-coupling. However, the $R_n$ value could not be increased too much beyond 10 $\Omega$ as the $I_c$ value and, therefore, the $I_cR_n$ value would decrease significantly. We are continuously optimizing the parameters of our step-edge Josephson junctions in order to maximize the $R_n$ and $I_cR_n$ values that are suitable for specified operating frequencies and temperatures.

The results presented here were obtained using liquid helium in the cryostat; the temperature at the device is estimated to be $\sim$10 K. Illuminating the detector with

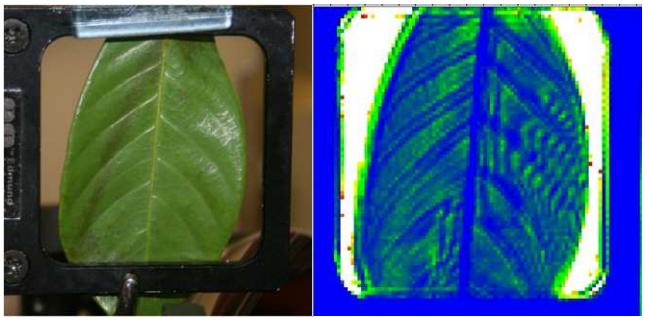

**Figure 5.** Mounted leaf sample (left) and THz image of the leaf (right).

0.6 THz radiation (under the same weakly-coupled power) did not produce a measurable response when cooled with liquid nitrogen (77 K). This was due to the small $V_c$ value (80 $\mu$V) of the detector and, therefore, a low characteristic frequency $f_c$ ($\sim$40 GHz) at 77 K. A study by Chen *et al* [12] showed that HTS Josephson junctions respond to a very broad frequency band but the maximum response is at a signal frequency $f_s \sim 2f_c$ [12]. Because the cryostat did not have a temperature controller, we were unable to verify whether the device was in fact more sensitive at 60 K, as suggested by figure 2(b) where $V_c = 600\ \mu$V and $f_c \approx 300$ GHz. However, such an operating temperature would be easily achieved with a relatively cheap one-stage cryocooler.

Figure 5 shows a THz transmission image of a leaf, which was acquired in 20 min. An area 5 cm $\times$ 5 cm was scanned at 0.5 mm resolution, giving an image size of $100 \times 100$ or 10 000 pixels. The integration time was 20 ms per pixel. However, a further 100 ms was required to position the stage and request the information. The leaf image demonstrates one of the key THz features, its sensitivity to water, with higher water content leaf veins showing higher attenuation.

Figure 6 shows a THz transmission image (also acquired in 20 min with the same scan points) of a chocolate bar in wrap with a metallic blade inserted inside. The text written on the chocolate and the blade are clearly visible in the THz image, even though they are not optically visible through the packaging. This observation clearly demonstrates the ability of THz radiation to see through packaging materials and reveal concealed items. This suggests that potential applications of THz imaging may be the detection of metallic contaminants in food through packaging materials.

The quality of the image is influenced by the source power and the detector noise, which includes the Josephson noise and bias current noise in the junction, and amplifier noise in the room temperature electronics. In this experiment, the maximum voltage response acquired by the lock-in amplifier with the optical chopper 'on' was $\sim$13 mV. The noise floor, measured when the THz source was completely blocked and the XY motor stage was stationary, was $\sim$1 $\mu$V. This gives a signal-to-noise ratio (SNR) $>$10 000 or 40 dB and a noise equivalent power NEP $\approx 1.67 \times 10^{-11}$ W Hz$^{-1/2}$ (corresponding to a voltage sensitivity of 12 000 V W$^{-1}$ and a bandwidth of 25 Hz). The SNR and NEP were limited by the room temperature electronics rather than the intrinsic noise of the Josephson detector (for noise in HTS Josephson


**Figure 6.** Optical photos of the wrapped chocolate bar with a metallic blade inserted (upper picture) and the text on the chocolate (lower left), and THz image of the chocolate bar (lower right).

junctions, see, for example, [20]). In addition, we observed during the sample scanning that the movement of the linear motor caused mechanical vibration (jittering) of the cryostat due to an unstable cryostat stage. This adds additional voltage noise which degrades the image quality. By comparing the acquired blocked and unblocked signal amplitudes, the SNR for the images presented here is approximately 18 dB.

Further work is under way to characterize and optimize the detector performance and reduce the additional noise sources caused by mechanical vibration and the room temperature electronics. In particular, we are working towards obtaining an HTS detector operating at liquid nitrogen temperature by optimizing our step-edge junction characteristics so that a compact, portable and cost-efficient imaging system can be realized. Design and implementation of an array configuration of such detectors will also be trialled to improve the scanning time and resolution.

## 5. Conclusion

We have successfully designed, fabricated and demonstrated a THz detector based on a ring-slot antenna-coupled HTS step-edge Josephson junction. An image system was constructed to test the detector's ability to generate images at 0.6 THz. The images acquired show the sensitivity of THz radiation to water content, and the capability of penetrating packaging materials to reveal concealed items. The work has demonstrated the potential of using the HTS Josephson junction device as a sensitive THz detector for imaging at higher operating temperature than that of the LTS devices.

## Acknowledgments

We thank Dr C P Foley for taking the SEM image of the step-edge junction, and Mr J Y Tello, P R Sullivan and R A Binks for their technical support.

## References


[1] For review paper, see for example Ferguson B and Zhang X C 2002 Materials for terahertz science and technology *Nat. Mater.* **1** 26–32

[2] Richard P 1994 Bolometers for infrared and millimetre waves *J. Appl. Phys.* **76** 1–24

[3] Luukanen A, Hadfield R H, Miller A J and Grossman E N 2004 A superconducting antenna-coupled microbolometer for THz applications *Proc. SPIE* **5411** 121–6

[4] Luukanen A, Miller A J and Grossman E N 2005 Passive hyperspectral terahertz imagery for security screening using a cryogenic microbolometer *Proc. SPIE* **5789** 127–34

[5] Ariyoshi S, Otani C, Dobroiu A, Sato H, Kawase K, Shimizu H M, Taino T and Matsuo H 2006 Terahertz imaging with a direct detector based on superconducting tunnel junctions *Appl. Phys. Lett.* **88** 203503

[6] Ariyoshi S, Otani C, Dobroiu A, Matsuo H, Sato H, Taino T, Kawase K and Shimizu H M 2006 Superconducting detector array for terahertz imaging applications *Japan. J. Appl. Phys.* **45** L1004–6

[7] Rosenthal P A and Grossman E N 1994 Terahertz Shapirosteps in high temperature SNS Josephson junctions *IEEE Trans. Microw. Theory Tech.* **42** 707–14

[8] Kislinskii Y V, Constantinian K Y, Borisenko I V, Ovsyannikov G A and Yagoubov P 2002 Submillimeter wave signal detection by bicrystal YBCO Josephson junctions at liquid nitrogen temperatures *Physica* C **372–376** 436–9

[9] Miyadera T, Kawayama I, Kiwa T, Tsukada K and Tonouchi M 2005 Frequency detection of focused sub-THz waves using a high-$T_c$ Josephson junction *Physica* C **426–431** 1726–30

[10] Lyatti M, Divin Y, Volkov O, Pavlovskii V, Gubankov V and Urban K 2007 Signal and noise characteristics of terahertz frequency-selective and broadband high-$T_c$ Josephson detectors *IEEE Trans. Appl. Supercond.* **17** 332–5

[11] Stepantsov E, Tarasov M, Kalabukhov A, Kuzmin L and Claeson T 2004 THz Josephson properties of grain boundary YBaCuO junctions on symmetric, tilted bicrystal sapphire substrates *J. Appl. Phys.* **96** 3357–61

[12] Chen J, Kurigata Y, Wang H B, Nakajima K, Yamashita T and Wu P H 2003 Wideband frequency metrology using high temperature superconducting Josephson junctions *IEEE Trans. Appl. Supercond.* **13** 1143–6

[13] Kaestner A, Volk M, Lugwig F, Schilling M and Menzel J 2000 $YBa_2Cu_3O_7$ Josephson junctions on $LaAlO_3$ bicrystals for terahertz-frequency applications *Appl. Phys. Lett.* **77** 1057–3059

[14] Humphreys R, Hirst P, Heath R, Elliner D, Parker N and Smith M A G 2004 Passive mm-wave imager using HTS Josephson junction detectors *Proc. SPIE* **5619** 59–69

[15] Foley C P, Mitchell E E, Lam S K H, Sankrithyan B, Wilson Y M, Tilbrook D L and Morris S J 1999 Fabrication and characterization of YBCO single grain boundary step edge junctions *IEEE Trans. Appl. Supercond.* **9** 4281–4

[16] Du J and Foley C P 2003 Trimming, stability and passivation of YBCO step-edge junctions *Physica* C **391** 31–41

[17] Du J, Lam S K H and Tilbrook D L 2001 Metallization and interconnection of HTS YBCO thin film devices and circuits *Supercond. Sci. Technol.* **14** 820–5

[18] Hellicar A, Du J, Nikolic N, Li L, Greene K, Beeton N, Hanham S, Kot J and Hislop G 2007 Development of a terahertz imaging system *Proc. IEEE Proc. Antennas and Propagation Int. Symp.* pp 5535–8

[19] Hesler J L and Crowe T W 2007 NEP and responsivity of THz zero-bias Schottky diode detectors *Infrared Millimeter Wave, 2007 and the 2007 15th Intern. Conf. on Terahertz Electronics IRMMW-THz, September 2007* pp 844–5

[20] Hao L, Macfarlane J C and Pegrum C M 1996 Excess noise in $YBa_2CuO_7$ thin film grain boundary Josephson junctions and devices *Supercond. Sci. Technol.* **9** 678–87